5

Concurrent wet and dry hydrological extremes at the global scale

Paolo De Luca[1,2,3], Gabriele Messori[2,4], Robert L. Wilby[1], Maurizio Mazzoleni[2,3] and Giuliano Di Baldassarre[2,3]

10

[1]Geography and Environment, Loughborough University, Loughborough, LE113TU, United Kingdom

[2]Department of Earth Sciences, Uppsala University, Uppsala, 75236, Sweden

[3]Centre of Natural Hazards and Disaster Science (CNDS), Uppsala, 75236, Sweden

[4]Department of Meteorology, Stockholm University and Bolin Centre for Climate Research, Stockholm, 10691, Sweden

15

Correspondence: Paolo De Luca (p.deluca@lboro.ac.uk) ORCID: https://orcid.org/0000-0002-0416-4622

Abstract. Multi-hazard events can be associated with larger socio-economic impacts than single-hazard events. Understanding
20 the spatio-temporal interactions characterising the former is, therefore, of relevance to disaster risk reduction measures. Here, we consider two high-impact hazards, namely wet and dry hydrological extremes, and quantify their global co-occurrence. We define these using the monthly self-calibrated Palmer Drought Severity Index based on the Penman-Monteith model (sc_PDSI_pm) covering the period 1950-2014, at 2.5° horizontal resolution. We find that the land areas affected by extreme wet, dry and wet-dry events (i.e. geographically remote, yet temporally co-occurring wet or dry extremes) all display increasing
25 trends with time, of which changes in dry and wet-dry episodes are significant (*p*-value <<0.01). The most geographically widespread wet-dry event covered a combined land area of 21 million km^2, with documented high-impact flooding and drought episodes spanning diverse regions. To further elucidate the interplay of wet and dry extremes at a grid-point scale, we introduce two new metrics: the wet-dry (WD) ratio and the extreme transition (ET) time interval. The WD-ratio measures the relative occurrence of extreme wet or dry events, whereas ET quantifies the average separation time of hydrological extremes with
30 opposite signs. The WD-ratio shows that the incidence of extreme wet episodes dominates over dry episodes in the USA, northern and southern south America, northern Europe, north Africa, western China and most of Australia. Conversely, extreme dry events are more prominent in most of the remaining regions. The median ET for wet to dry is ~27 months, while the dry to wet median ET is 21 months. We also evaluate correlations between wet-dry hydrological extremes and leading

modes of large-scale variability, namely the: El Niño–Southern Oscillation (ENSO), Pacific Decadal Oscillation (PDO) and American Multi-decadal Oscillation (AMO). We find that ENSO and PDO have a similar influence globally, with the former significantly impacting (p-value <0.05) a larger area compared to the latter, whereas the AMO shows an almost inverse pattern, and significantly impacts a larger overall area. Our analysis brings new insights on hydrological multi-hazards and are of direct relevance to governments and organisations with globally distributed interests, such as (re)insurance companies. Specifically, the multi-hazard maps may be used to evaluate worst-case disaster scenarios considering the potential co-occurrence of wet and dry hydrological extremes.

Keywords: multi-hazards; PDSI; wet-dry; metrics; hydrological extremes

10

1 Introduction

Natural hazards can interact in diverse ways, leading to multi-hazard events that can exacerbate disaster losses when compared to single-hazard occurrences (Zscheischler et al., 2018). Examples of multi-hazards are the co-occurrence of flooding with wind damage from extra-tropical cyclones (De Luca et al., 2017), storm surge combined with fluvial flooding in deltas (Ward et al., 2018), flood episodes along with droughts (Collet et al., 2018) and landslides triggered by earthquakes (Kargel et al., 2016). Such combinations can lead to situations beyond the worst-case scenario planned by emergency managers, (re)insurance companies, businesses and governments and thus present a critical challenge for disaster risk reduction (Zscheischler et al., 2018). The relevance of multi-hazards has been recognised by both the scientific and stakeholder communities – both have devoted significant efforts to the topic over the past decade (e.g. Forzieri et al., 2016; Gallina et al., 2016; Gill and Malamud, 2014; Kappes et al., 2012; Terzi et al., 2019; Zscheischler et al., 2018). Indeed, the United Nations Sendai Framework for Disaster Risk Reduction (UNISDR, 2015) now advocates multi-hazard approaches to disaster risk reduction.

Analysis of multi-hazards is highly relevant given anthropogenic climate change. Events such as floods and droughts already have significant socio-economic impacts (Barredo, 2007; Jonkman, 2005; Naumann et al., 2015; Zhang et al., 2011), and are expected to become more frequent and/or severe in the future (Dai, 2012, 2011; Hirabayashi et al., 2013; Milly et al., 2002). Numerous studies have investigated the combination of flood and drought events or, more generally, wet and dry hydrological extremes at local and regional scales, for both present and future climates (e.g. Di Baldassarre et al., 2017; Berton et al., 2017; Collet et al., 2018; Deangelis et al., 1984; Gil-Guirado et al., 2016; Oni et al., 2016; Parry et al., 2013; Pechlivanidis et al., 2017; Quesada-Montano et al., 2018; Yan et al., 2013; Yoon et al., 2018). Examples include the analysis of abrupt drought-flood transitions in river basins in China (Yan et al., 2013) and in England and Wales (Parry et al., 2013), but also the dynamical interplay between society and hydrological extremes (Di Baldassarre et al., 2017) and indices assessing the long-term evolution of vulnerability and adaptation to both floods and droughts (Gil-Guirado et al., 2016). Other studies consider wet-dry

interactions from a statistical perspective (Collet et al., 2018), or have related these two hazards to large-scale modes of climate variability (Cai and Rensch, 2012; Lee et al., 2018; Nobre et al., 2017; Siegert et al., 2001; Ward et al., 2014; Yoon et al., 2018).

5   Quantifying wet and dry (also extreme) hydrological events at both regional and global scales is a non-trivial task. Some commonly used indicators include the Palmer Drought Severity Index (PDSI) (Dai et al., 2004; Palmer, 1965), the Standardized Precipitation Index (SPI) (McKee et al., 1995, 1993) and the Standardized Precipitation Evapotranspiration Index (SPEI) (Vicente-Serrano et al., 2010). For instance, the PDSI was used to evaluate the combined effect of the Pacific Decadal Oscillation (PDO) and El Niño Southern Oscillation (ENSO) on global wet and dry changes over land, showing that when
10   these two modes are in phase (e.g. El Niño-warm PDO) wet and dry events are amplified (Wang et al., 2014). The PDSI and SPEI have also been used to quantify wet and dry trends over China (Rubel and Kottek, 2010), with a generally good agreement between the two (Chen et al., 2017). At the global scale, the SPI and SPEI were used to explore wet and dry links with ENSO, PDO and the North Atlantic Oscillation (NAO) (Sun et al., 2016). The study found that ENSO has the greatest spatial impact for wet and dry changes, followed by the PDO having an effect in the American continent and eastern Russia, and the NAO
15   affecting Europe as well as north Africa. Lastly, the SPI was also used in a global multi-model ensemble study of future projections in pluvial and drought events (Martin, 2018). This revealed that more severe pluvial events are expected in already wet regions and the same applies for more severe drought conditions in dry areas.

     In this study we adopt a relatively broad definition of multi-hazard events, including both the temporal (yet spatially separate)
20   co-occurrence of wet and dry hydrological extremes at the global scale, and the rapid succession of hydrological extremes of opposite sign at the same location. We emphasize that the term "hydrological extreme" does not necessarily imply *observed* flooding or drought events, unless explicitly mentioned. The relevance of both types of multi-hazards is evident. Stakeholders with geographically diverse portfolios, such as international corporations and (re)insurance companies, need to have a robust understanding of the co-occurrence statistics of natural hazards. They also need to account for the occurrence of damaging
25   events in rapid succession, whose compound impacts may exceed the linear sum of the expected impacts for isolated wet and dry extremes. Similarly, estimates of the range of times that intervene between the two different extremes can inform disaster preparedness and prevention measures. Finally, national economies that are sensitive to agricultural output can be impacted by the occurrence of sequential hydrological extremes (Zampieri et al., 2017; Zhang et al., 2015).

30   Notwithstanding their socio-economic relevance, concurrent wet and dry hydrological extreme events at the global scale have seldom been addressed in the literature. One early study did consider combinations of wet and dry extremes via observed PDSI for two thresholds (wet, PDSI > 3 and dry, PDSI < -3) (Dai et al., 2004). This showed that the total global land area (60°S-75°N) impacted by wet-dry extremes increased between 1950 and 2002, with marked changes occurring from the early 1970s and surface warming being attributed to these changes after the mid-1980s. We extend this analysis by: i) using an updated

3

time series (1950-2014); ii) introducing new metrics for assessing concurrent wet-dry extremes; iii) presenting findings at monthly rather than annual resolution; and above all iv) defining the most geographically-widespread multi-hazard events, occurring within each month, instead of simply considering extreme observations with PDSI > 3 and PDSI < -3. We explore these multi-hazard properties using the monthly self-calibrated PDSI dataset (Dai, 2017; Sheffield et al., 2012). We specifically address the following questions:

i)   What were the most geographically-widespread extreme wet, dry and concurrent wet-dry events?

ii)   To what extent were these wet-dry PDSI extremes associated with documented flood and drought episodes?

iii)   How frequent were extreme wet or dry events in the past?

iv)   What is the most likely time interval between opposing extremes at a given location?

v)   How wet and dry extremes are linked with predominant modes of climate variability?

2 Data and Methods

2.1 Data

We use the self-calibrated monthly-mean Palmer Drought Severity Index based on the Penman-Monteith model (sc_PDSI_pm) (Dai, 2017; Sheffield et al., 2012) for the 1950-2014 period, at 2.5° horizontal resolution. Self-calibration enables a more consistent comparison between different climatic regions, and the Penman-Monteith model outperforms the original PDSI Thornthwaite algorithm (Wells et al., 2004) in representing potential evaporation at the global scale (Sheffield et al., 2012). From this dataset, we obtain extreme wet and dry monthly observed events by filtering the data respectively for sc_PDSI_pm $\geq$ 3 and sc_PDSI_pm $\leq$ -3. These two thresholds represent *very moist spells* and *severe droughts*. Only grid-cells with time series having $\geq$ 95% of observations over the period of interest are considered.

We further analyse three climate modes of variability known to affect regional and global precipitation patterns: the Niño3.4 (Rayner et al., 2003; Trenberth, 1997), PDO (Mantua and Hare, 2002) and Atlantic Multidecadal Oscillation (AMO) (Schlesinger and Ramankutty, 1994). All these climate indices are at monthly time-resolution from 1950 to 2014, as issued by the National Oceanic & Atmospheric Administration (NOAA).

2.2 Methods for identifying extreme wet, dry, neutral and wet-dry events

First we calculate the percentage of total land area impacted by the most widespread monthly extreme wet (sc_PDSI_pm $\geq$ 3) and dry (sc_PDSI_pm $\leq$ -3) hydrological events along with neutral (-3 < sc_PDSI_pm < 3) and extreme wet plus extreme dry events within the period 1950-2014. Monthly extreme wet events were calculated following De Luca et al. (2017) by: (i) computing the wet annual maxima (AMAX), i.e. the highest sc_PDSI_pm observations within each calendar year, at each grid-cell, (ii) counting the number of wet AMAX observations by date, and (iii) taking the extreme wet event with the most

geographically-widespread impacts, i.e. largest impacted area (km^2), within each month during 1950-2014. Extreme dry events were calculated in a similar way to extreme wet events except that in place of AMAX the sc_PDSI_pm annual minima (AMIN), i.e. the lowest sc_PDSI_pm observations within each year, were used to compute the extreme events. Neutral events were identified as follows: i) extract the sc_PDSI_pm AMAX of (non-extreme) wet events ($0 \leq$ sc_PDSI_pm < 3); ii) extract the

5 sc_PDSI_pm AMIN for (non-extreme) dry events ($-3 <$ sc_PDSI_pm < 0); iii) pool within the same dataset both (non-extreme) wet/dry AMAX/AMIN events by month; iv) compute the most widespread neutral events by month as per above. Lastly, concurrent extreme wet-dry events were calculated by summing their relative impacted areas (%) within each month. A Mann-Kendall test (Kendall, 1975; Mann, 1945) was performed to assess any significant trends within each time series. Relative Sen's slopes (Sen, 1968) with *p*-values were also computed.

10

Second, to establish whether the most widespread extreme wet, dry and wet-dry events were solely due to chance, a boot-strapping analysis of n=10,000 samples was performed from the original sc_PDSI_pm dataset. The boot-strapping's steps were as follows: i) prepare the complete global (i.e. all grid-cells) sc_PDSI_pm dataset from 1950 to 2014; ii) sample, with replacement, the sc_PDSI_pm values n=10,000 times from this global dataset; iii) calculate n=10,000 extreme wet and

15 n=10,000 extreme dry events with the same algorithm used above with the original dataset; iv) take the impacted area of the most geographically-widespread wet and dry events for each sample; v) calculate the mean and corresponding 95% confidence intervals (c.i.) for the extreme wet and extreme dry events. Statistical significance was assessed by checking whether observed extreme wet or dry % of total impacted areas fell outside the 95% c.i. of the boot-strapped means. If this was the case, the observations were considered statistically significant.

20

2.3 Wet-dry metrics

The *wet-dry (WD) ratio* is derived on a cell by cell basis by taking the natural logarithm of the total number of extreme wet observations (months with sc_PDSI_pm ≥ 3) divided by the total number of extreme dry observations (months with sc_PDSI_pm ≤ -3) over the 1950-2014 period:

25

$$WD - ratio_h = \ln\left(\sum_{i=1}^{n_i} Wet_{i,h} \Big/ \sum_{j=1}^{n_j} Dry_{j,h}\right) \qquad (1)$$

where h refers to a single grid-cell and n_i and n_j are the total number of wet and dry events, respectively. The WD-ratio gives information about the propensity of a given area to be more affected by wet or dry extremes. Thus, WD-ratio > 0 signifies that

30 wet extremes outnumber dry extremes and WD-ratio < 0 indicates a predominance of dry extremes over wet ones. The natural logarithm was used to narrow the range of WD-ratio values and to separate the wet-dominated versus dry-dominated regions by sign. As a caveat, we note that the WD ratio does not account for the different intensities of wet and dry extremes.

Wet to dry and *dry to wet* transitions, here named *extreme transitions* (ET) were assessed for each grid-cell by computing the average time interval (months) between these events, within the 1950-2014 period. More specifically, ET for wet to dry was derived as follows, for each grid-cell: i) extract both wet (sc_PDSI_pm $\geq$ 3) and dry (sc_PDSI_pm $\leq$ -3) extreme observations

5   from the entire (1950-2014) sc_PDSI_pm dataset; ii) order observations by time, from oldest to the most recent; iii) retain only the earliest event in the case of consecutive extreme dry observations and the latest in the case of consecutive wet observations; iv) calculate the time interval (monthly difference) between wet and dry observations within the time-series; and v) take the average of the time interval. The same algorithm was applied for calculating ET from dry to wet for each grid-cell, with the only difference being in step iii) where the earliest wet and latest dry observations are kept and in step iv) where the time

10   interval is now calculated between dry to wet transitions.

To check the statistical significance of the observed ET, a boot-strapping analysis with n = 1,000 samples (10,000 samples were not possible due to high computational demand) was performed in a similar way as for the most widespread extreme wet, dry and wet-dry events. Here, for each grid-cell, the following steps were followed: i) from the main sc_PDSI_pm dataset

15   extract and flag extreme wet (sc_PDSI_pm $\geq$ 3) and extreme dry (sc_PDSI_pm $\leq$ -3) observations; ii) sample, with replacement, n=1,000 of these wet and dry observations with the corresponding (sampled) date (year-month); iii) calculated n=1,000 ET from wet to dry and n=1,000 ET from dry to wet using the same algorithm as per above; and iv) take the ET (wet to dry and dry to wet) means with the relative 95% c.i. of the means. Statistical significance was assessed by checking, for each grid-cell, if the observed ET time interval (wet to dry and dry to wet) mean fell outside the 95% c.i. of the boot-strapped

20   ET mean. If this was the case the observation was considered statistically significant.

2.4 Correlation with Climate Indices

Associations between extreme wet-dry hydrological extremes and the three modes of climate variability (Niño3.4, PDO and AMO) were assessed using Spearman's rank correlation test. Specifically, the correlations were performed for each grid-cell

25   using monthly wet and dry extreme observations (sc_PDSI_pm $\geq$ 3 and sc_PDSI_pm $\leq$ -3) paired with the corresponding monthly values of Niño3.4, PDO and AMO. Spearman's test does not require data to be normally distributed, which is the case for the wet-dry extreme PDSI values. The wet-dry extreme datasets were computed, for each grid-cell, by adding together the extreme wet and dry monthly observations within the 1950-2014 period. Since the number of correlation tests performed is large (> 2,700) there is a risk of incurring in statistically significant results simply by chance. Thus, to account for Type I

30   errors (or 'false positives') the Bonferroni correction (Bonferroni, 1936; Sedgwick, 2014) was applied to all *p*-values.

Finally, since Niño3.4 may affect correlations with other modes of climate variability, we removed this signal from the PDO and AMO by performing partial correlations, with the R programming package 'ppcor' (see documentation here: https://cran.r-project.org/web/packages/ppcor/ppcor.pdf) (Kim, 2015). Partial correlations can be seen as the relationship between two

random variables after removing the effect of one or more other random variables. Here the partial correlations, between two variables x_i (e.g. PDO) and x_j (e.g. sc_PDSI_pm) given a third variable x_k (e.g. Niño3.4) is defined as follows (Kim, 2015; Whittaker, 2009):

$$r_{ij|k} = \frac{r_{ij} - r_{ik}r_{jk}}{\sqrt{1 - r_{ik}^2}\sqrt{1 - r_{jk}^2}} \qquad (2)$$

In this study we computed the partial correlations, using the Spearman's correlation coefficient, for PDO and AMO, given the Niño3.4, with respect to sc_PDSI_pm extreme wet and dry observations.

3. Results

3.1 Land area impacted by extreme wet, dry, neutral and wet-dry events

The percentage (%) of total global land area impacted by the most widespread extreme wet, dry and neutral events is shown in Figure 1, at monthly resolution from 1950 to 2014. For extreme wet events (Figure 1a, sc_PDSI_pm $\geq$ 3) the average impacted area over the 65-year period is 2.17%. The most widespread wet event occurred in December 2010 (7.77%, discussed in section 3.2). The Mann-Kendall test indicates a positive, though non-significant trend (with Sen's slope = 1.6e-04). The rise in extreme wet area is consistent with previous work (Dai et al., 2004).

For extreme dry events (Figure 1b, sc_PDSI_pm $\leq$ -3) the average area is 2.38% and the largest event occurred in January 2003 (8.57%, discussed in section 3.2). In this case, the Mann-Kendall test indicates a positive and statistically significant (*p*-value <<0.01) trend (with Sen's slope = 1.7e-03). This signifies that the total area subject to severe drought increased between 1950 and 2014. This result agrees with previous studies showing a global increase in drought risk, attributed to anthropogenic climate change, in both observations and climate model simulations (Dai, 2012, 2011; Dai et al., 2004; Marvel et al., 2019). Such changes in drought are linked to anomalies in tropical sea surface temperatures (SSTs) and therefore driven by both El Niño and La Niña phases, along with increased surface warming from the 1980s.

The most widespread neutral events (Figure 1c, -3 < sc_PDSI_pm < 3) affect on average 13.64% of the global land area over the 1950-2014 period. The Mann-Kendall test shows a negative and significant (*p*-value <<0.01) trend (with Sen's slope = -1.9e-03). Such a reduction in the area under neutral conditions is counteracted by the observed increasing trend of both extreme wet and dry events. The neutral events show strong seasonality, with peaks of impacted area occurring during December. This resembles what is seen for the most widespread wet and dry events, which also tend to occur mostly during boreal winter.

However, the fact that 73.4% of the global sc_PDSI_pm land area is in the northern hemisphere may introduce a bias in the result.

Finally, the area with concurrent wet-dry hydrological extremes (Figure 1d) shows an increasing (Sen's slope = 1.08e-03) and statistically significant (p-value <<0.01) trend, again in agreement with shorter records (Dai et al., 2004). The mean monthly value of total global area with concurrent wet-dry extremes is 4.56%.
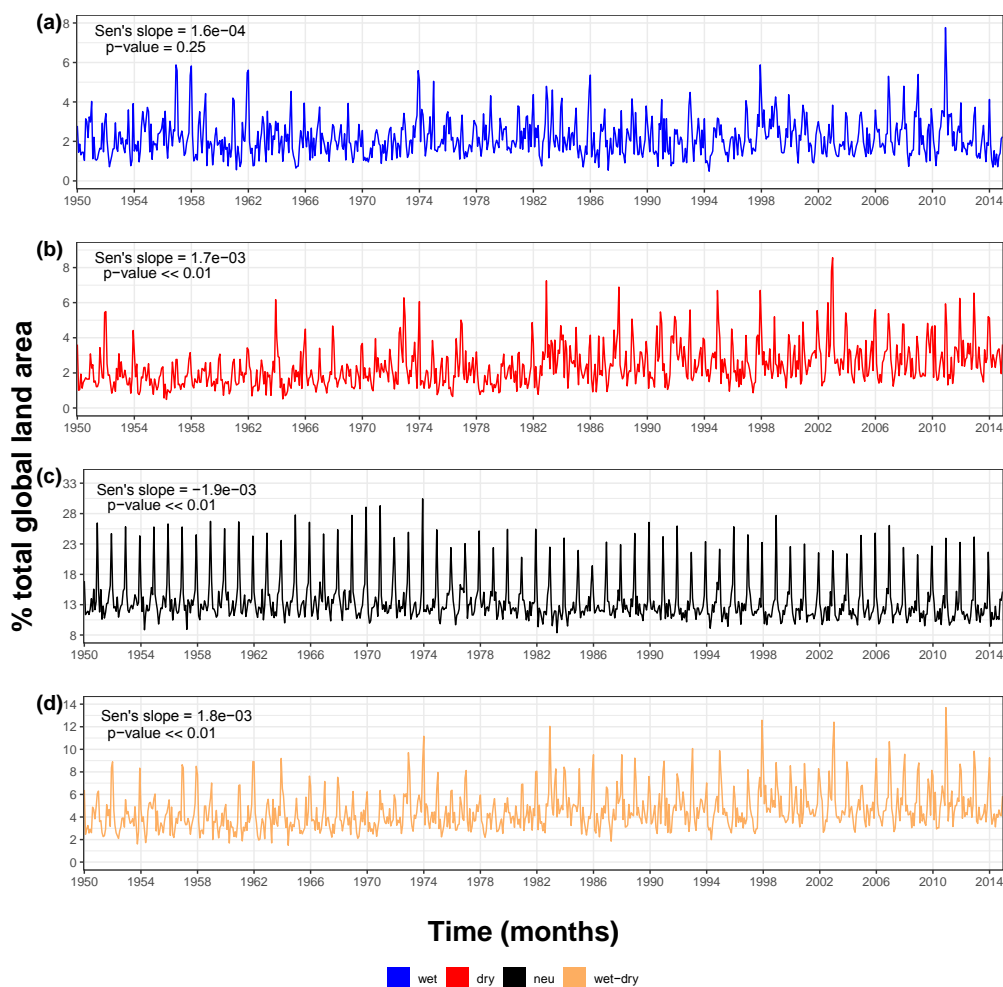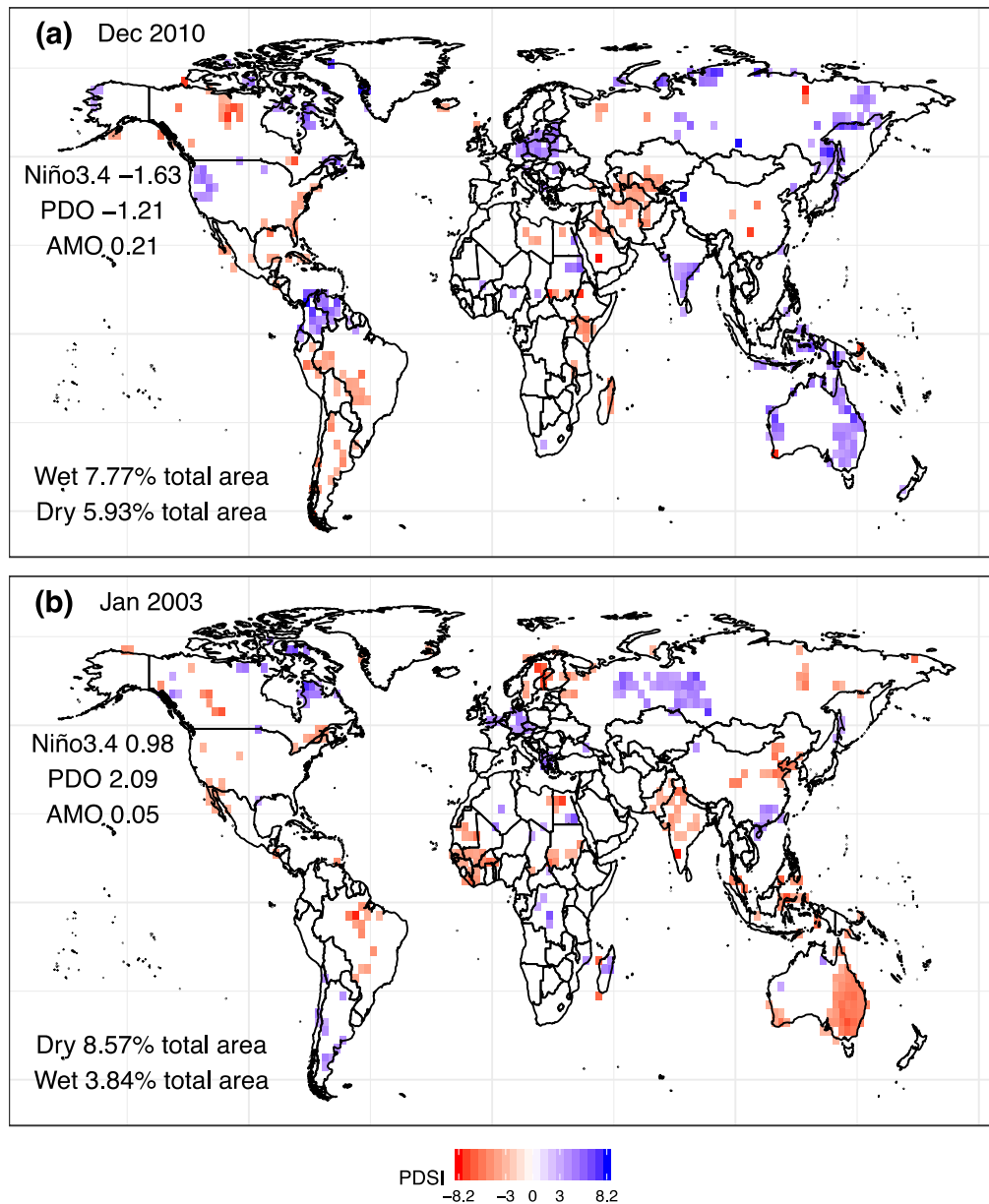

Figure 1. Percentage (%) of total land area with **(a)** wet (blue) and **(b)** dry (red) extremes along **(c)** neutral (black) and **(d)** extreme wet + extreme dry (orange) events over the 1950-2014 period. Wet extremes are sc_PDSI_pm $\geq$ 3) and dry extremes sc_PDSI_pm $\leq$ -3 monthly observations. Sen's slopes and the significance of the Mann Kendall test (p-values) are shown in each panel.

3.2 Concurrent global flood and drought events

We next consider the single most extensive wet, wet-dry and dry events, and show that they capture recorded severe drought and flood events around the world. The most widespread global extreme wet event was also the most widespread wet-dry event, and it occurred in December 2010 (Figure 2a). Recorded events matching this occurrence include the devastating Queensland floods in Australia (BBC, 2010a; Smith et al., 2013; Trenberth and Fasullo, 2012; Zhong et al., 2013), heavy floods and landslides occurring in south-east India killing more than 180 people (Reliefweb, 2010), widespread flooding and landslides over Colombia and Venezuela causing about 300 deaths and leaving thousands homeless (BBC, 2010b; Telegraph, 2010; Trenberth and Fasullo, 2012) and flooding affecting the north-western USA (NWRFC, 2010). Severe wet conditions were also recorded in central-eastern Europe, however no significant damages were reported by the media. Such a widespread wet event impacted 7.77% of the total global land area. December 2010 was characterized by a very strong negative Niño3.4 phase, within the 2010-2012 La Niña event (Luo et al., 2017). Moreover, the PDO and AMO were respectively in their cold and positive phases. The same phases occurred during November 2010 (not shown), and these antecedent conditions may have contributed to the extreme wet and dry events in the sc_PDSI_pm series (Lee et al., 2018). At the same time, droughts were recorded in central Asia, Madagascar, the Horn of Africa (BBC, 2011), south America, eastern USA (NOAA, 2011) and north Canada, covering a total of 5.93% of land area. Both the extreme wet and dry percentages (%) of land area impacted are significantly different from their respective values expected by chance (95% c.i.).

The most widespread extreme dry hydrological event occurred during January 2003 with 8.57% of total land area impacted by drought and 3.84% of land experiencing wet hydrological extremes and floods (Figure 2b). During this event, eastern Australia was the most affected region, experiencing the worst drought in 20 years, which was driven by an El Niño event that lead to severe dust storms and bushfires (Gabric et al., 2010; Horridge et al., 2005; Levinson and Waple, 2004; McAlpine et al., 2007). This episode belongs to the so called 'Millennium Drought' (Van Dijk et al., 2013) which affected Australia between 2001 and 2009. Other regions experiencing severe drought during January 2003 were north-east China, India (Sinha et al., 2016), Scandinavia (Irannezhad et al., 2017), west Africa, parts of Brazil and a few scattered areas between Mexico, USA, Canada, Russia and Indonesia. January 2003 was an El Niño month with the Niño3.4 index being in a positive phase at the same time as a warm PDO phase. On the other hand, the AMO registered an almost neutral phase. As for the December 2010 episode in Figure 2a, such climate patterns occurred also in the previous month. Meanwhile, other regions experienced wet hydrological extremes and floods, such as south-east China, central Russia, Europe, southern Great Britain (BBC, 2003; Marsh, 2004), Madagascar (Reliefweb, 2003), Argentina, Chile and scattered parts of Africa and Canada (DFO, 2008). The % of land area impacted by both extreme wet and dry events during January 2003 was significantly different from the value expected by chance (95% c.i.).

Figure 2. (a) Most widespread extreme global wet hydrological event (blue colour) and coincident extreme dry areas (red colour), December 2010. The event was also the most widespread concurrent wet-dry episode. The percentage (%) of total land area is shown for both wet and dry extremes, along with the values of the three climate indices (i.e. Niño3.4, PDO and AMO) in December 2010. **(b)** As **(a)** but for the most widespread extreme global dry hydrological event, January 2003. **(a)-(b)** The analysis is based on the self-calibrated monthly mean Palmer Drought Severity Index (sc_PDSI_pm) for the period 1950-2014.

10

3.3 Wet-dry (WD) ratio

The WD-ratio highlights regions that experienced higher or lower frequencies of wet or dry hydrological extremes (Figure 3). The patterns identified here represent the 65-year propensity for more or less extreme wet or extreme dry events in a given area. Hot spots for extreme wet tendency emerge in the USA, northern Mexico, Colombia, Venezuela, Argentina, Bolivia, Paraguay, northern Europe, North Africa, eastern China and Australia. On the other hand, regions with higher frequencies of extreme dry events are found in Canada, central south America, central and southern Europe/Africa, western China and south-western Australia. Other regions, such as Russia, display mixed patterns. These WD-ratio patterns are in agreement with global trends in drought over the 1950-2010 period, identified using the sc_PDSI_pm dataset (Dai, 2012).
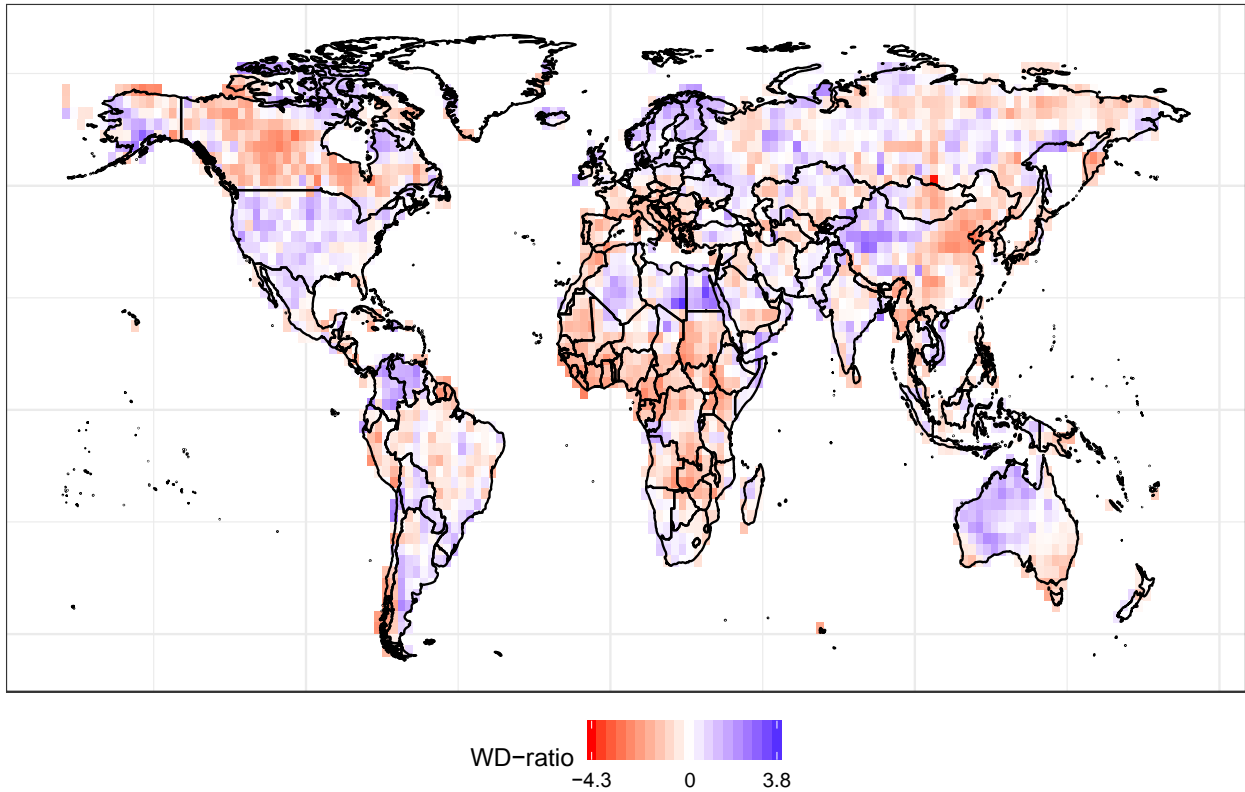

Figure 3. Wet-dry (WD) ratio derived for every grid-cell. Blue colours (WD-ratio > 0) mean that the area experienced more wet than dry hydrological extremes. Red colours (WD-ratio < 0) indicate the opposite.

11

3.4 Extreme transitions (ET)

In Figure 4a we show the extreme transitions (ET), in time interval (months), from wet to dry and dry to wet extreme events within the period 1950-2014 plotted against the percentage of total land area impacted. The ET from wet to dry (blue curve) exhibits a peak at 22-months with 4.3% of total land having this mean time interval. On the other hand, ET from dry to wet (red curve) peaks at 18-month with almost 5% of global land having this average separation time. Overall, ET from wet to dry takes longer than ET from dry to wet. According to the boot-strap analysis, the ET for wet to dry extremes are statistically significant in all grid-cells; for dry to wet only 10 grid-cells are not different from chance. We also show the cumulative distribution functions (CDFs) of wet to dry and dry to wet ET time intervals (Figure 4b). For wet to dry 50% of the ET occur within ~27 months, whereas for dry to wet 50% of ET are observed within 21 months. The two ET distributions are significantly different (p-value <<0.01, Mann-Whitney-Wilcoxon test) under the null hypothesis that their means are equal.

Moreover, ET from dry to dry and wet to wet were also computed (not shown). Dry to dry time intervals peak at 27 months with 3.21% of land area impacted, whereas wet to wet time intervals peak at 30 months with 3.14% of area affected. For dry to dry ET 50% occurred within ~37 months and the same but for wet to wet ET in ~36 months. A Mann-Whitney-Wilcoxon test shows that the two distributions are significantly different (p-value <0.01), under the null hypothesis that their means are equal as per the multi-hazards case.
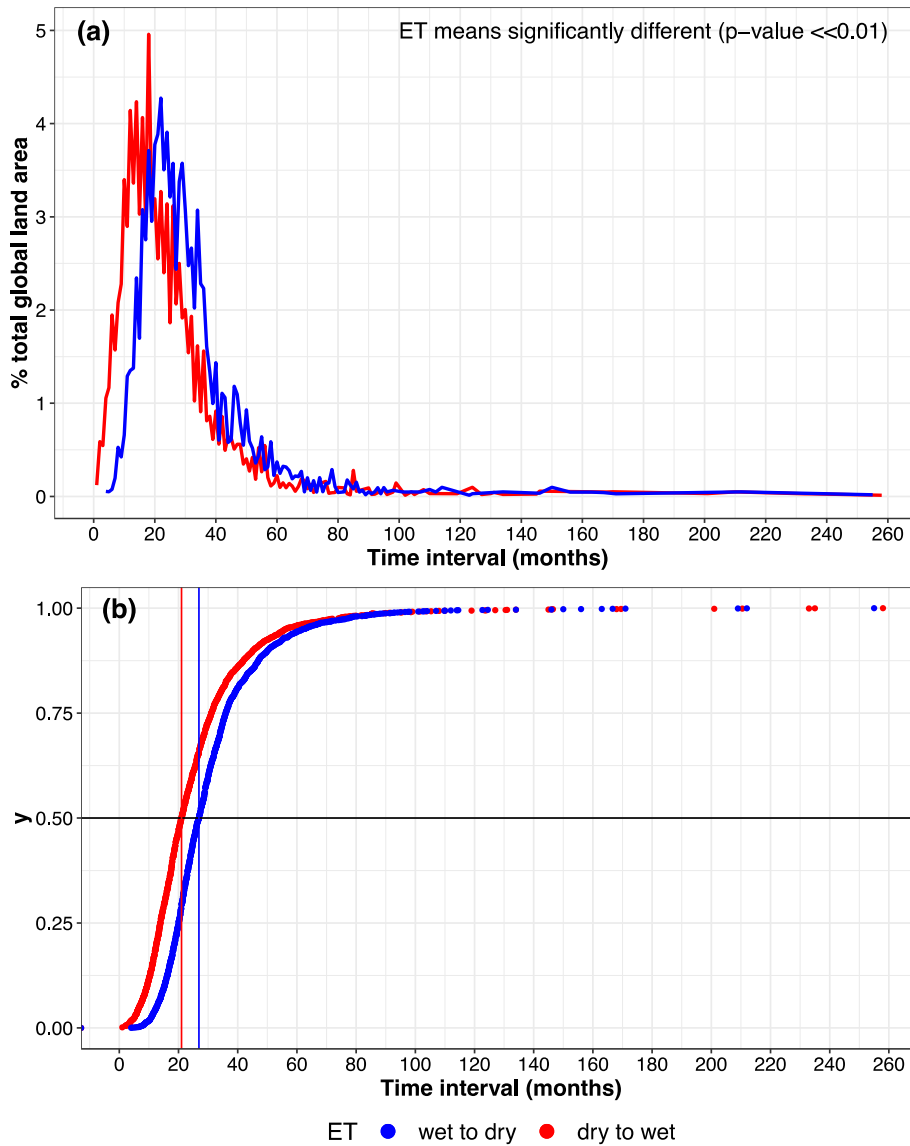
Figure 4. Extreme transition (ET) time intervals between extreme wet to dry (blue) and between extreme dry to wet (red). **(a)** ET as a function of the total percentage (%) of total land area impacted and **(b)** cumulative distribution functions (CDFs). The horizontal black line in (b) indicates the 50th quantile (i.e. median) of the distribution and the blue and red lines the respective ET time intervals. The two distributions show a statistically significant difference in their means (p-value $<<0.01$, Mann-Whitney-Wilcoxon test).

13

3.5 Correlations with climate indices

In Figure 5 we show global correlations between hydrological extremes (wet and dry) and the three major modes of climate variability (Niño3.4, PDO and AMO), which are known to have a significant effect on regional precipitation/temperature patterns and hence flood and drought events. Details of the calculation are provided in Section 2.4. We also computed the same correlation tests for the NAO (Barnston and Livezey, 1987), Pacific North-American (PNA) pattern (Barnston and Livezey, 1987) and Quasi-Biennial Oscillation (QBO) (Baldwin et al., 2001), however very few correlations were statistically significant (not shown).

ENSO is one of the modes with the most widespread global impacts and is here represented by the Niño3.4 index (Figure 5a). The positive phase of Niño3.4 (which can lead to El Niño events), is negatively correlated (p-value <0.05) with extreme wet sc_PDSI_pm values over parts of central Canada, northern South America, southern Africa, India, central China, central and northern Russia, Indonesia and eastern Australia. On the other hand, positive and significant correlations are found over southern USA, in some scattered regions of central and southern south-America and in the Middle East. This implies that a positive Niño3.4 phase is associated with a lower likelihood of extreme wet hydrological events (sc_PDSI_pm $\geq$ 3) in these regions, whereas negative Niño3.4 phase (possibly leading to La Niña events) typically enhances such extremes.

In Figure 5b-c we show global partial correlations between hydrological extremes, measured with sc_PDSI_pm, and PDO/AMO modes of climate variability with the ENSO signal removed. Correlations for PDO (Figure 5b) generally resemble the spatial patterns found for Niño3.4. Here, negative correlations are also found in north-western North-America, equatorial Africa and eastern Russia. At the same time, almost all significant correlations over Australia, China and India vanish. On the other hand, positive correlations are found in central-western USA, southern South-America and Kazakhstan. The fact that Niño3.4 and PDO correlations show very similar spatial patterns (Figures 5a and 5b) suggests that when these two indices are in phase (i.e. El Niño-warm PDO and La Niña-cold PDO), wet and dry changes are magnified (Wang et al., 2014). The correlation pattern shown in Figure 5b also agrees with season-ahead peak river flow correlations with the PDO (Lee et al., 2018).

The pattern of AMO correlations (Figure 5c) differs from Niño3.4 and PDO indices and returns a greater number of significant (p-value <0.05) grid-boxes than Niño3.4 (2.5% more grid-cells overall). For the AMO, negative and significant correlations are found in Brazil, Argentina, Mexico, scattered areas in north America, the Horn of Africa and eastern China. Positive correlations are found in the Sahel region of Africa, Russia and central Asia. Our results are again in agreement with global season-ahead correlations found between peak river flows and AMO (Lee et al., 2018).
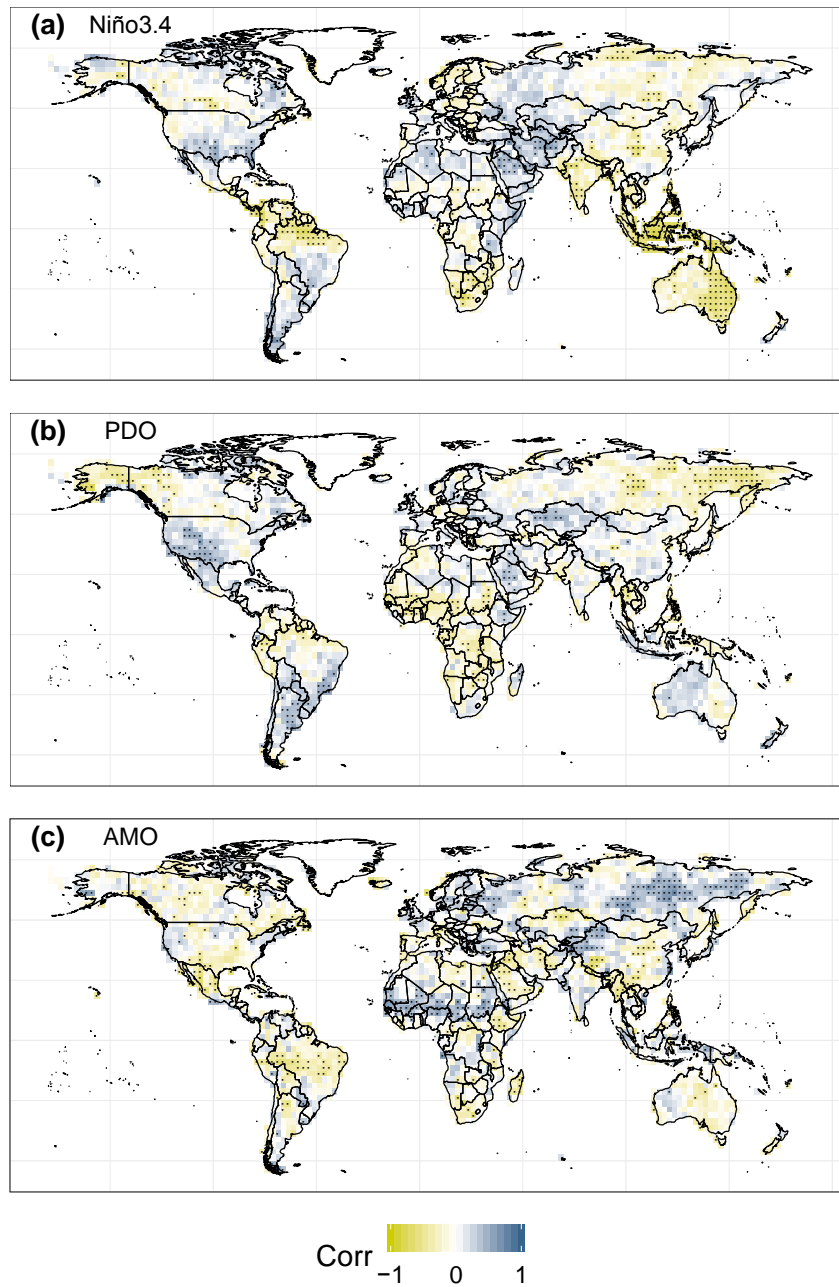
Figure 5. Correlations between extreme wet (sc_PDSI_pm ≥ 3) and dry (sc_PDSI_pm ≤ -3) hydrological events and **(a)** Niño3.4, **(b)** PDO and **(c)** AMO. For **(b)** and **(c)** partial correlations are performed to remove the Niño3.4 signal. Correlations and partial correlations make use of the Spearman's correlation coefficient. Correlations significant at the 5% level (p-value <0.05) are shown by stippling. The Bonferroni correction was applied to all p-values. In (b) and (c) the ENSO signal has been removed via partial correlations.

4. Discussion and Conclusions

Natural hazards, such as wet and dry extremes, can coincide over time and space creating multi-hazard events in turn leading to significant socio-economic losses. Geographically remote co-occurring extremes pose a potential economic risk to stakeholders with global assets and/or supply chains. For instance, knowledge of recurrent patterns of coincident hydrological
5   extremes could be used to hedge losses, in regional hydropower production (Ng et al., 2017; Turner et al., 2017) and/or with respect to crop yield (Leng and Hall, 2019; Xie et al., 2018; Zampieri et al., 2017), planting and harvesting (Sacks et al., 2010). Rapid successions of extremes at the same location pose challenges for disaster preparedness, management and risk reduction. Floods and droughts are expected to become more frequent and severe in the future due to anthropogenic climate change (Arnell and Gosling, 2016; Dai, 2012; Hirabayashi et al., 2013; IPCC, 2012), underscoring the importance of research on
10   multi-hazard hydrological extremes.

In this study we investigated a range of multi-hazard hydrological extremes at the global scale during the period 1950 to 2014, with the primary objective of identifying the most geographically-widespread events. Our secondary goal was to develop new metrics for describing some of the properties of wet-dry extremes, namely combinations of wet and dry extremes at locations,
15   or their succession at a given location. We found that the land area affected by extreme dry and geographically remote wet-dry events has increasing and statistically significant trends. This coincides with the expectation that such hazards are set to increase (Güneralp et al., 2015; Hirabayashi et al., 2013), and is in agreement with previous studies (Dai, 2012; Dai et al., 2004). In the present work, however, we applied a more stringent definition of extreme events (De Luca et al., 2017), which captures well-known flooding and drought episodes. We further showed that these extremes can have global-scale impacts, by
20   giving emphasis to the most widespread wet, dry and wet-dry events.

We further introduced two new metrics, the wet-dry (WD) ratio and the extreme transition (ET) between wet/dry and dry/wet extremes. The former discerns the local predominance of extreme wet or extreme dry events, by considering both types of extremes simultaneously. Areas experiencing more wet than dry extremes were detected in the USA, northern and southern
25   South-America, northern Europe and North Africa, western China and most of Australia. More dry than wet extremes were experienced in most of the remaining areas. Such knowledge, although based on historical observations, could raise awareness amongst emergency planners, (re)insurance companies, farmers, relief organizations, and international agencies to better plan and adapt to extreme wet and dry hydrological events. The ET metric estimates for every grid-cell the average time interval between opposing extremes (i.e. transitions from wet to dry and from dry to wet). Our results show that the two ET time-series'
30   means differ significantly (p-value $<<0.01$) and that ET between wet to dry are on average slower than dry to wet (22- *versus* 18-month interval on average). Knowing long-term changes in ET time intervals between wet to dry and dry to wet hydrological extremes can be significant for emergency planners, local businesses, governments and stakeholders. For example, if average intervals shorten, losses could accrue more frequently, causing recurrent shocks to local economies and, in some regions, impeding development.

16

The analysis was based on the self-calibrated monthly-mean Palmer Drought Severity Index. Future research opportunities include the use of other indices, such as the Standardized Precipitation Index (McKee et al., 1995, 1993) or the Standardized Precipitation Evapotranspiration Index (Vicente-Serrano et al., 2010) to validate our findings and to account for uncertainty in the observations of concurrent wet-dry extremes. Emphasis should also be given to evaluating the seasonality of the extremes, as more robust and meaningful patterns could emerge, specifically with respect to correlations with modes of climate variability. Similar analyses could be applied to single Köppen climate zones (Rubel and Kottek, 2010) to discern possible regional variations in concurrent wet-dry extreme characteristics. Finally, once baseline maps and data for hydrological multi-hazards have been established from observations, the next step could be to investigate with climate model output how these phenomena may change under anthropogenic climate change.

To this end, it is important to identify possible climate drivers of the observed hydrological extremes. In this study, we computed correlations between wet-dry hydrological extremes and the corresponding values of the ENSO, PDO and AMO indices. The global correlation patterns for ENSO confirm previous studies (Emerton et al., 2017; Lee et al., 2018; Wang et al., 2014; Ward et al., 2014), that investigated the effect of both El Niño and La Niña events on global flood hazard and global season-ahead correlations between river peak flows and climate indices, such as ENSO, PDO and AMO. We further highlight that ENSO-induced wet and dry changes are magnified when in phase with the PDO index. Global correlations are found between the sc_PDSI_pm and PDO/AMO too. The PDO patterns generally match those of ENSO, and this confirms the finding that when ENSO and PDO are in phase they amplify the global wet and dry changes (Wang et al., 2014). The AMO, however, shows different and in some cases opposite correlation patterns when compared to ENSO and PDO. Correlations of hydrological extremes with modes of climate variability can be helpful for seasonal and sub-seasonal hydrological forecasting and, in this case, they provide information about what kind of climate index phase is driving wet and dry extremes in different regions globally. They also point to physical mechanisms, linked to climate dynamics, which may have not been uncovered yet.

Author contribution

PDL conceived the methods, performed the analyses, created the pictures and wrote the first manuscript draft. GM and RW contributed to the methods. All the authors contributed to the writing.

5

15

20

25

30

References

Arnell, N.W., Gosling, S.N., 2016. The impacts of climate change on river flood risk at the global scale. Clim. Change 134, 387–401. https://doi.org/10.1007/s10584-014-1084-5

Baldwin, M.P., Gray, L.J., Dunkerton, T.J., Hamilton, K., Haynes, P.H., Randel, W.J., Holton, J.R., Alexander, M.J., Hirota, I., Horinouchi, T., Jones, D.B.A., Kinnersley, J.S., Marquardt, C., Sato, K., Takahashi, M., 2001. The quasi-biennial oscillation. Rev. Geophys. 39, 179–229. https://doi.org/10.1029/1999RG000073

Barnston, A.G., Livezey, R.E., 1987. Classification, Seasonality and Persistence of Low-Frequency Atmospheric Circulation Patterns. Mon. Weather Rev.

Barredo, J.I., 2007. Major flood disasters in Europe: 1950–2005. Nat. Hazards 42, 125–148. https://doi.org/10.1007/s11069-006-9065-2

BBC, 2011. Horn of Africa sees "worst drought in 60 years." https://www.bbc.co.uk/news/world-africa-13944550.

BBC, 2010a. Australia: Queensland floods spur more evacuations. https://www.bbc.co.uk/news/world-asia-pacific-12097280.

BBC, 2010b. Colombia flooding continues with thousands homeless. https://www.bbc.co.uk/news/world-latin-america-12006568.

BBC, 2003. Floods bring miserable start to 2003. http://news.bbc.co.uk/1/hi/uk/2623729.stm.

Berton, R., Driscoll, C.T., Adamowski, J.F., 2017. The near-term prediction of drought and flooding conditions in the northeastern United States based on extreme phases of AMO and NAO. J. Hydrol. 553, 130–141. https://doi.org/https://doi.org/10.1016/j.jhydrol.2017.07.041

Bonferroni, C., 1936. Teoria statistica delle classi e calcolo delle probabilita. Pubbl. del R Ist. Super. di Sci. Econ. e Commericiali di Firenze 8, 3–62.

Cai, W., Rensch, P., 2012. The 2011 southeast Queensland extreme summer rainfall: A confirmation of a negative Pacific Decadal Oscillation phase? Geophys. Res. Lett. 39. https://doi.org/10.1029/2011GL050820

Chen, T., Zhang, H., Chen, X., Hagan, D.F., Wang, G., Gao, Z., Shi, T., 2017. Robust drying and wetting trends found in regions over China based on Köppen climate classifications. J. Geophys. Res. Atmos. 122, 4228–4237. https://doi.org/10.1002/2016JD026168

Collet, L., Harrigan, S., Prudhomme, C., Formetta, G., Beevers, L., 2018. Future hot-spots for hydro-hazards in Great Britain: a probabilistic assessment. Hydrol. Earth Syst. Sci. 22, 5387–5401. https://doi.org/10.5194/hess-22-5387-2018

Dai, A., 2017. Dai Global Palmer Drought Severity Index (PDSI). https://doi.org/10.5065/D6QF8R93

Dai, A., 2012. Increasing drought under global warming in observations and models. Nat. Clim. Chang. 3, 52.

Dai, A., 2011. Drought under global warming: A review. Wiley Interdiscip. Rev. Clim. Chang. 2, 45–65. https://doi.org/10.1002/wcc.81

Dai, A., Trenberth, K.E., Qian, T., 2004. A Global Dataset of Palmer Drought Severity Index for 1870–2002: Relationship with Soil Moisture and Effects of Surface Warming. J. Hydrometeorol. 5, 1117–1130. https://doi.org/10.1175/JHM-386.1

De Luca, P., Hillier, J.K., Wilby, R.L., Quinn, N.W., Harrigan, S., 2017. Extreme multi-basin flooding linked with extra-tropical cyclones. Environ. Res. Lett. 12, 114009.

Deangelis, R.J., Urban, J.B., Gburek, W.J., Contino, M.A., 1984. Precipitation and runoff on eight New England basins during extreme wet and dry periods. Hydrol. Sci. J. 29, 13–28. https://doi.org/10.1080/02626668409490919

5 DFO, 2008. Dartmouth Flood Observatory, Global Active Archive of Large Flood Events [WWW Document]. http://www.dartmouth.edu/~floods/Archives/2003sum.htm.

Di Baldassarre, G., Martinez, F., Kalantari, Z., Viglione, A., 2017. Drought and flood in the Anthropocene: feedback mechanisms in reservoir operation. Earth Syst. Dyn. 8, 225–233. https://doi.org/10.5194/esd-8-225-2017

Emerton, R., Cloke, H.L., Stephens, E.M., Zsoter, E., Woolnough, S.J., Pappenberger, F., 2017. Complex picture for likelihood
10 of ENSO-driven flood hazard. Nat. Commun. 8, 14796.

Forzieri, G., Feyen, L., Russo, S., Vousdoukas, M., Alfieri, L., Outten, S., Migliavacca, M., Bianchi, A., Rojas, R., Cid, A., 2016. Multi-hazard assessment in Europe under climate change. Clim. Change 137, 105–119. https://doi.org/10.1007/s10584-016-1661-x

Gabric, A.J., Cropp, R.A., McTainsh, G.H., Johnston, B.M., Butler, H., Tilbrook, B., Keywood, M., 2010. Australian dust
15 storms in 2002–2003 and their impact on Southern Ocean biogeochemistry. Global Biogeochem. Cycles 24. https://doi.org/10.1029/2009GB003541

Gallina, V., Torresan, S., Critto, A., Sperotto, A., Glade, T., Marcomini, A., 2016. A review of multi-risk methodologies for natural hazards: Consequences and challenges for a climate change impact assessment. J. Environ. Manage. 168, 123–132.

20 Gil-Guirado, S., Espín-Sánchez, J.-A., Del Rosario Prieto, M., 2016. Can we learn from the past? Four hundred years of changes in adaptation to floods and droughts. Measuring the vulnerability in two Hispanic cities. Clim. Change 139, 183–200. https://doi.org/10.1007/s10584-016-1768-0

Gill, J.C., Malamud, B.D., 2014. Reviewing and visualizing the interactions of natural hazards. Rev. Geophys. 52, 680–722. https://doi.org/10.1002/2013RG000445

25 Güneralp, B., Güneralp, İ., Liu, Y., 2015. Changing global patterns of urban exposure to flood and drought hazards. Glob. Environ. Chang. 31, 217–225. https://doi.org/https://doi.org/10.1016/j.gloenvcha.2015.01.002

Hirabayashi, Y., Mahendran, R., Koirala, S., Konoshima, L., Yamazaki, D., Watanabe, S., Kim, H., Kanae, S., 2013. Global flood risk under climate change. Nat. Clim. Chang. 3, 816.

Horridge, M., Madden, J., Wittwer, G., 2005. The impact of the 2002–2003 drought on Australia. J. Policy Model. 27, 285–
30 308. https://doi.org/https://doi.org/10.1016/j.jpolmod.2005.01.008

IPCC, 2012. Managing the Risks of Extreme Events and Disasters to Advance Climate Change Adaptation. A Special Report of Working Groups I and II of the Intergovernmental Panel on Climate Change. Cambridge University Press, Cambridge, UK, and New York, NY, USA. https://doi.org/10.1017/CBO9781139177245

Irannezhad, M., Ahmadi, B., Kløve, B., Moradkhani, H., 2017. Atmospheric circulation patterns explaining climatological

drought dynamics in the boreal environment of Finland, 1962–2011. Int. J. Climatol. 37, 801–817. https://doi.org/10.1002/joc.5039

Jonkman, S.N., 2005. Global perspectives on loss of human life caused by floods. Nat. Hazards 34, 151–175. https://doi.org/10.1007/s11069-004-8891-3

Kappes, M.S., Keiler, M., von Elverfeldt, K., Glade, T., 2012. Challenges of analyzing multi-hazard risk: a review. Nat. Hazards 64, 1925–1958. https://doi.org/10.1007/s11069-012-0294-2

Kargel, J.S., Leonard, G.J., Shugar, D.H., Haritashya, U.K., Bevington, A., Fielding, E.J., Fujita, K., Geertsema, M., Miles, E.S., Steiner, J., Anderson, E., Bajracharya, S., Bawden, G.W., Breashears, D.F., Byers, A., Collins, B., Dhital, M.R., Donnellan, A., Evans, T.L., Geai, M.L., Glasscoe, M.T., Green, D., Gurung, D.R., Heijenk, R., Hilborn, A., Hudnut, K., Huyck, C., Immerzeel, W.W., Liming, J., Jibson, R., Kääb, A., Khanal, N.R., Kirschbaum, D., Kraaijenbrink, P.D.A., Lamsal, D., Shiyin, L., Mingyang, L., McKinney, D., Nahirnick, N.K., Zhuotong, N., Ojha, S., Olsenholler, J., Painter, T.H., Pleasants, M., Pratima, K.C., Yuan, Q.I., Raup, B.H., Regmi, D., Rounce, D.R., Sakai, A., Donghui, S., Shea, J.M., Shrestha, A.B., Shukla, A., Stumm, D., van der Kooij, M., Voss, K., Xin, W., Weihs, B., Wolfe, D., Lizong, W., Xiaojun, Y., Yoder, M.R., Young, N., 2016. Geomorphic and geologic controls of geohazards induced by Nepal's 2015 Gorkha earthquake. Science (80-.). 351.

Kendall, M., 1975. Multivariate analysis. Griffin, London.

Kim, S., 2015. ppcor: An R Package for a Fast Calculation to Semi-partial Correlation Coefficients. Commun. Stat. Appl. methods 22, 665–674. https://doi.org/10.5351/CSAM.2015.22.6.665

Lee, D., Ward, P., Block, P., 2018. Attribution of Large-Scale Climate Patterns to Seasonal Peak-Flow and Prospects for Prediction Globally. Water Resour. Res. 54, 916–938. https://doi.org/10.1002/2017WR021205

Leng, G., Hall, J., 2019. Crop yield sensitivity of global major agricultural countries to droughts and the projected changes in the future. Sci. Total Environ. 654, 811–821. https://doi.org/https://doi.org/10.1016/j.scitotenv.2018.10.434

Levinson, D.H., Waple, A.M., 2004. STATE OF THE CLIMATE IN 2003. Bull. Am. Meteorol. Soc. 85, S1–S72.

Luo, J.-J., Liu, G., Hendon, H., Alves, O., Yamagata, T., 2017. Inter-basin sources for two-year predictability of the multi-year La Niña event in 2010–2012. Sci. Rep. 7, 2276. https://doi.org/10.1038/s41598-017-01479-9

Mann, H.B., 1945. Nonparametric Tests Against Trend. Econometrica 13, 245–259. https://doi.org/10.2307/1907187

Mantua, N.J., Hare, S.R., 2002. The Pacific Decadal Oscillation. J. Oceanogr. 58, 35–44. https://doi.org/10.1023/A:1015820616384

Marsh, T.J., 2004. The January 2003 flood on the Thames. Weather 59, 59–62. https://doi.org/10.1256/wea.212.03

Martin, E.R., 2018. Future Projections of Global Pluvial and Drought Event Characteristics. Geophys. Res. Lett. 45, 11,911-913,920. https://doi.org/10.1029/2018GL079807

Marvel, K., Cook, B.I., Bonfils, C.J.W., Durack, P.J., Smerdon, J.E., Williams, A.P., 2019. Twentieth-century hydroclimate changes consistent with human influence. Nature 569, 59–65. https://doi.org/10.1038/s41586-019-1149-8

McAlpine, C.A., Syktus, J., Deo, R.C., Lawrence, P.J., McGowan, H.A., Watterson, I.G., Phinn, S.R., 2007. Modeling the

impact of historical land cover change on Australia's regional climate. Geophys. Res. Lett. 34. https://doi.org/10.1029/2007GL031524

McKee, T.B., Doesken, N.J., Kleist, J., 1995. Drought monitoring with multiple time scales. Proc. 9th Conf. Appl. Climatol. 233–236. https://doi.org/10.1007/s13398-014-0173-7.2

McKee, T.B., Doesken, N.J., Kleist, J., 1993. The relationship of drought frequency and duration to time scales. AMS 8th Conf. Appl. Climatol. 179–184. https://doi.org/citeulike-article-id:10490403

Milly, P.C.D., Wetherald, R.T., Dunne, K.A., Delworth, T.L., 2002. Increasing risk of great floods in a changing climate. Nature 415, 514–517. https://doi.org/10.1038/415514a

Naumann, G., Spinoni, J., Vogt, J. V, Barbosa, P., 2015. Assessment of drought damages and their uncertainties in Europe. Environ. Res. Lett. 10, 124013.

Ng, J.Y., Turner, S.W.D., Galelli, S., 2017. Influence of El Niño Southern Oscillation on global hydropower production. Environ. Res. Lett. 12, 34010. https://doi.org/10.1088/1748-9326/aa5ef8

NOAA, 2011. State of the Climate: Drought for December 2010. https://www.ncdc.noaa.gov/sotc/drought/201012.

Nobre, G.G., Jongman, B., Aerts, J., Ward, P.J., 2017. The role of climate variability in extreme floods in Europe. Environ. Res. Lett. 12, 84012.

NWRFC, 2010. 2010 Northwest Floods. https://www.nwrfc.noaa.gov/floods/dec_2010/2010_Northwest_Flood.pdf 19.

Oni, S., Futter, M., Ledesma, J., Teutschbein, C., Buttle, J., Laudon, H., 2016. Using dry and wet year hydroclimatic extremes to guide future hydrologic projections. Hydrol. Earth Syst. Sci. 20, 2811–2825. https://doi.org/10.5194/hess-20-2811-2016

Palmer, W., 1965. Meteorological Drought. U.S. Res. Pap. No. 45. US Weather Bur. DC.

Parry, S., Marsh, T., Kendon, M., 2013. 2012: from drought to floods in England and Wales. Weather 68, 268–274. https://doi.org/10.1002/wea.2152

Pechlivanidis, I.G., Arheimer, B., Donnelly, C., Hundecha, Y., Huang, S., Aich, V., Samaniego, L., Eisner, S., Shi, P., 2017. Analysis of hydrological extremes at different hydro-climatic regimes under present and future conditions. Clim. Change 141, 467–481. https://doi.org/10.1007/s10584-016-1723-0

Quesada-Montano, B., Di Baldassarre, G., Rangecroft, S., Van Loon, A.F., 2018. Hydrological change: Towards a consistent approach to assess changes on both floods and droughts. Adv. Water Resour. 111, 31–35. https://doi.org/https://doi.org/10.1016/j.advwatres.2017.10.038

Rayner, N.A., Parker, D.E., Horton, E.B., Folland, C.K., Alexander, L. V, Rowell, D.P., Kent, E.C., Kaplan, A., 2003. Global analyses of sea surface temperature, sea ice, and night marine air temperature since the late nineteenth century. J. Geophys. Res. Atmos. 108. https://doi.org/10.1029/2002JD002670

Reliefweb, 2010. India: Floods - Dec 2010. https://reliefweb.int/disaster/fl-2010-000249-ind.

Reliefweb, 2003. Madagascar: Floods - Jan 2003. https://reliefweb.int/disaster/fl-2003-0037-mdg.

Rubel, F., Kottek, M., 2010. Observed and projected climate shifts 1901-2100 depicted by world maps of the Köppen-Geiger

climate classification. Meteorol. Zeitschrift 19, 135–141. https://doi.org/10.1127/0941-2948/2010/0430

Sacks, W.J., Deryng, D., Foley, J.A., Ramankutty, N., 2010. Crop planting dates: an analysis of global patterns. Glob. Ecol. Biogeogr. 19, 607–620. https://doi.org/10.1111/j.1466-8238.2010.00551.x

Schlesinger, M.E., Ramankutty, N., 1994. An oscillation in the global climate system of period 65-70 years. Nature 367, 723–726. https://doi.org/10.1038/367723a0

Sedgwick, P., 2014. Multiple hypothesis testing and Bonferroni's correction. BMJ Br. Med. J. 349, g6284. https://doi.org/10.1136/bmj.g6284

Sen, P.K., 1968. Estimates of the Regression Coefficient Based on Kendall's Tau. J. Am. Stat. Assoc. 63, 1379–1389. https://doi.org/10.1080/01621459.1968.10480934

Sheffield, J., Wood, E.F., Roderick, M.L., 2012. Little change in global drought over the past 60 years. Nature 491, 435.

Siegert, F., Ruecker, G., Hinrichs, A., Hoffmann, A.A., 2001. Increased damage from fires in logged forests during droughts caused by El Niño. Nature 414, 437–440. https://doi.org/10.1038/35106547

Sinha, D., Syed, T.H., Famiglietti, J.S., Reager, J.T., Thomas, R.C., 2016. Characterizing Drought in India Using GRACE Observations of Terrestrial Water Storage Deficit. J. Hydrometeorol. 18, 381–396. https://doi.org/10.1175/JHM-D-16-0047.1

Smith, J.K.G., Young, M.M., Wilson, K.L., Craig, S.B., 2013. Leptospirosis following a major flood in Central Queensland, Australia. Epidemiol. Infect. 141, 585–590.

Sun, Q., Miao, C., AghaKouchak, A., Duan, Q., 2016. Century-scale causal relationships between global dry/wet conditions and the state of the Pacific and Atlantic Oceans. Geophys. Res. Lett. 43, 6528–6537. https://doi.org/10.1002/2016GL069628

Telegraph, 2010. Floods devastate Colombia and Venezuela. https://www.telegraph.co.uk/news/worldnews/southamerica/colombia/8186408/Floods-devastate-Colombia-and-Venezuela.html.

Terzi, S., Torresan, S., Schneiderbauer, S., Critto, A., Zebisch, M., Marcomini, A., 2019. Multi-risk assessment in mountain regions: A review of modelling approaches for climate change adaptation. J. Environ. Manage. 232, 759–771. https://doi.org/https://doi.org/10.1016/j.jenvman.2018.11.100

Trenberth, K.E., 1997. The Definition of El Niño. Bull. Am. Meteorol. Soc. 78, 2771–2778.

Trenberth, K.E., Fasullo, J.T., 2012. Climate extremes and climate change: The Russian heat wave and other climate extremes of 2010. J. Geophys. Res. Atmos. 117. https://doi.org/10.1029/2012JD018020

Turner, S.W.D., Hejazi, M., Kim, S.H., Clarke, L., Edmonds, J., 2017. Climate impacts on hydropower and consequences for global electricity supply investment needs. Energy 141, 2081–2090. https://doi.org/https://doi.org/10.1016/j.energy.2017.11.089

UNISDR, 2015. Sendai Framework for Disaster Risk Reduction 2015 - 2030. Third World Conf. Disaster Risk Reduction, Sendai, Japan, 14-18 March 2015. 1–25. https://doi.org/A/CONF.224/CRP.1

Van Dijk, A.I.J.M., Beck, H.E., Crosbie, R.S., De Jeu, R.A.M., Liu, Y.Y., Podger, G.M., Timbal, B., Viney, N.R., 2013. The Millennium Drought in southeast Australia (2001-2009): Natural and human causes and implications for water resources, ecosystems, economy, and society. Water Resour. Res. 49, 1040–1057. https://doi.org/10.1002/wrcr.20123

Vicente-Serrano, S.M., Beguería, S., López-Moreno, J.I., 2010. A Multiscalar Drought Index Sensitive to Global Warming: The Standardized Precipitation Evapotranspiration Index. J. Clim. 23, 1696–1718. https://doi.org/10.1175/2009JCLI2909.1

Wang, S., Huang, J., He, Y., Guan, Y., 2014. Combined effects of the Pacific Decadal Oscillation and El Niño-Southern Oscillation on Global Land Dry–Wet Changes. Sci. Rep. 4, 6651.

Ward, P.J., Couasnon, A., Eilander, D., Haigh, I.D., Hendry, A., Muis, S., Veldkamp, T.I.E., Winsemius, H.C., Wahl, T., 2018. Dependence between high sea-level and high river discharge increases flood hazard in global deltas and estuaries. Environ. Res. Lett. 13, 84012. https://doi.org/10.1088/1748-9326/aad400

Ward, P.J., Jongman, B., Kummu, M., Dettinger, M.D., Sperna Weiland, F.C., Winsemius, H.C., 2014. Strong influence of El Niño Southern Oscillation on flood risk around the world. Proc. Natl. Acad. Sci. 111, 15659–15664.

Wells, N., Goddard, S., Hayes, M.J., 2004. A Self-Calibrating Palmer Drought Severity Index. J. Clim. 17, 2335–2351.

Whittaker, J., 2009. Graphical Models in Applied Multivariate Statistics. Wiley Publishing.

Xie, W., Xiong, W., Pan, J., Ali, T., Cui, Q., Guan, D., Meng, J., Mueller, N.D., Lin, E., Davis, S.J., 2018. Decreases in global beer supply due to extreme drought and heat. Nat. Plants 4, 964–973. https://doi.org/10.1038/s41477-018-0263-1

Yan, D.H., Wu, D., Huang, R., Wang, L.N., Yang, G.Y., 2013. Drought evolution characteristics and precipitation intensity changes during alternating dry–wet changes in the Huang–Huai–Hai River basin. Hydrol. Earth Syst. Sci. 17, 2859–2871. https://doi.org/10.5194/hess-17-2859-2013

Yoon, J.-H., Wang, S.-Y.S., Lo, M.-H., Wu, W.-Y., 2018. Concurrent increases in wet and dry extremes projected in Texas and combined effects on groundwater. Environ. Res. Lett. 13, 54002. https://doi.org/10.1088/1748-9326/aab96b

Zampieri, M., Ceglar, A., Dentener, F., Toreti, A., 2017. Wheat yield loss attributable to heat waves, drought and water excess at the global, national and subnational scales. Environ. Res. Lett. 12, 64008. https://doi.org/10.1088/1748-9326/aa723b

Zhang, Q., Gu, X., Singh, V.P., Kong, D., Chen, X., 2015. Spatiotemporal behavior of floods and droughts and their impacts on agriculture in China. Glob. Planet. Change 131, 63–72.

Zhang, Q., Zhang, W., Chen, Y.D., Jiang, T., 2011. Flood, drought and typhoon disasters during the last half-century in the Guangdong province, China. Nat. Hazards 57, 267–278. https://doi.org/10.1007/s11069-010-9611-9

Zhong, S., Clark, M., Hou, X.-Y., Zang, Y.-L., FitzGerald, G., 2013. 2010–2011 Queensland floods: Using Haddon's Matrix to define and categorise public safety strategies. Emerg. Med. Australas. 25, 345–352.

Zscheischler, J., Westra, S., van den Hurk, B.J.J.M., Seneviratne, S.I., Ward, P.J., Pitman, A., AghaKouchak, A., Bresch, D.N., Leonard, M., Wahl, T., Zhang, X., 2018. Future climate risk from compound events. Nat. Clim. Chang. 8, 469–477. https://doi.org/10.1038/s41558-018-0156-3